QCD corrections and anomalous couplings in $Z\gamma$ production at hadron colliders

U. Baur

Department of Physics, State University of New York at Buffalo, Buffalo, New York 14260

T. Han

Department of Physics, University of California, Davis, California 95616
and Department of Physics, University of Wisconsin, Madison, Wisconsin 53706

J. Ohnemus

Lawrence Berkeley Laboratory, Berkeley, California 94720

The processes $p\overset{(-)}{p}\to Z\gamma+X\to\ell^+\ell^-\gamma+X$ ($\ell=e,\mu$) and $p\overset{(-)}{p}\to Z\gamma+X\to\bar{\nu}\nu\gamma+X$ are calculated to $\mathcal{O}(\alpha_s)$ for general $ZZ\gamma$ and $Z\gamma\gamma$ couplings. The impact of $\mathcal{O}(\alpha_s)$ QCD corrections on the observability of $ZZ\gamma$ and $Z\gamma\gamma$ couplings in $Z\gamma$ production at the Fermilab Tevatron and the CERN Large Hadron Collider (LHC) is discussed. [S0556-2821(98)01605-1]

PACS number(s): 12.38.Bx, 14.70.Fm, 14.70.Hp

I. INTRODUCTION

Experiments at high energy hadron colliders provide an excellent opportunity to probe the interactions of the electroweak gauge bosons. Recent observation of electroweak gauge boson pair production at the Fermilab Tevatron have provided further confirmation of the electroweak standard model (SM) and have significantly tightened the constraints on possible non-standard model self-interactions of the electroweak gauge bosons [1–5]. For instance, $W\gamma$ production [1,2] can be used to study the $WW\gamma$ vertex, WZ production can be used to probe the WWZ vertex, and W^+W^- production [3,4,6] is sensitive to both the $WW\gamma$ and WWZ vertex functions. Furthermore, efforts have also been made to search for evidence of nonzero $ZZ\gamma$ and $Z\gamma\gamma$ couplings in $Z(\to\ell^+\ell^-)\gamma$ ($\ell=e,\mu$) [5,7,8] and $Z(\to\bar{\nu}\nu)\gamma$ production [5,9]. These couplings vanish in the SM at the tree level. However, if new interactions beyond the SM are responsible for nonzero $ZZ\gamma$ or $Z\gamma\gamma$ couplings, then $Z\gamma$ production could provide a clean signal for new physics.

Previous studies of $ZZ\gamma$ and $Z\gamma\gamma$ couplings in hadronic $Z\gamma$ production were based on leading order calculations [10]. Next-to-leading order (NLO) calculations of $p\overset{(-)}{p}\to Z\gamma$ production in the SM have shown that the NLO corrections are largest at high values of the photon transverse momentum and high values of the $Z\gamma$ invariant mass [11,12]. These are the same regions of phase space where the effects of nonstandard $ZZ\gamma$ and $Z\gamma\gamma$ couplings are most pronounced [10]. It is therefore important to include NLO corrections when probing for evidence of nonstandard $ZZ\gamma$ and $Z\gamma\gamma$ couplings in hadronic $Z\gamma$ production. This paper presents a calculation of hadronic $Z(\to\ell^+\ell^-)\gamma$ and $Z(\to\bar{\nu}\nu)\gamma$ production to $\mathcal{O}(\alpha_s)$, including the most general nonstandard $ZZ\gamma$ and $Z\gamma\gamma$ couplings, and the decay of the Z boson in the narrow width approximation. Because of the larger $Z\to\bar{\nu}\nu$ branching ratio, the $Z(\to\bar{\nu}\nu)\gamma$ cross section is about a factor 3 larger than the combined $Z(\to e^+e^-)\gamma$ and $Z(\to\mu^+\mu^-)\gamma$ rates. This results in substantially better limits on anomalous $ZZ\gamma$ and $Z\gamma\gamma$ couplings in the $Z\to\bar{\nu}\nu$ channel [9].

To perform our calculation, we use the Monte Carlo method for NLO calculations described in Ref. [13]. In the calculation the SM is assumed to be valid apart from anomalies in the $ZZ\gamma$ and $Z\gamma\gamma$ vertices. In particular, we assume the couplings of W and Z bosons to quarks and leptons to be given by the SM, and that there are no nonstandard couplings of the $Z\gamma$ pair to two gluons [14]. The gluon fusion process, $gg\to Z\gamma$, is small in the SM [15] and is not considered in this paper. Section II briefly reviews the method used to carry out the calculation, and describes how anomalous $ZZ\gamma$ and $Z\gamma\gamma$ couplings are incorporated.

In Sec. III, we discuss how NLO QCD corrections influence the photon transverse momentum distribution, and derive sensitivity limits for nonstandard $ZZ\gamma$ and $Z\gamma\gamma$ couplings at NLO for the Tevatron and CERN Large Hadron Collider (LHC) center-of-mass energies for various integrated luminosities. The photon transverse momentum distribution is the observable most sensitive to anomalous couplings [10], and is used by the Collider Detector at Fermilab (CDF) and D0 to extract information on the $ZZ\gamma$ and $Z\gamma\gamma$ vertices [5,7–9]. At the Tevatron, QCD corrections are modest, and slightly improve the sensitivity bounds. In contrast, at LHC energies, the inclusive NLO QCD corrections are quite large at high photon transverse momenta in the SM and reduce the sensitivity to anomalous $ZZ\gamma$ and $Z\gamma\gamma$ couplings somewhat. The large QCD corrections are caused by a log squared enhancement factor in the $qg\to Z\gamma q$ partonic cross section at high photon transverse momentum (p_T), and the large quark-gluon luminosity at LHC energies. As in $W\gamma$ [16], WZ [17,18], and W^+W^- production [19,20], the effect of the QCD corrections at high p_T at the LHC can be reduced by imposing a 0-jet requirement when searching for anomalous couplings. Finally, summary remarks are given in Sec. IV.

II. OVERVIEW OF THE CALCULATION

The calculation presented here generalizes the results of Refs. [11] and [12] to include general (nonstandard model)
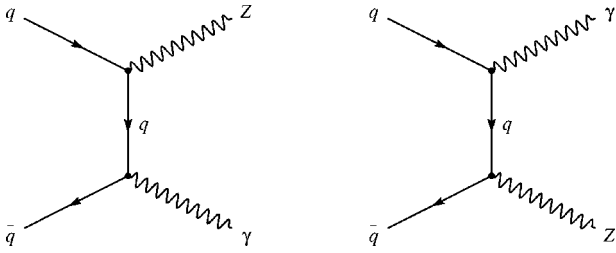
FIG. 1. Feynman diagrams for the Born level process $q\bar{q} \rightarrow Z\gamma$ in the standard model.

$ZZ\gamma$ and $Z\gamma\gamma$ couplings. The calculation employs a combination of analytic and Monte Carlo integration techniques; details of the method can be found in Ref. [13]. The leptonic Z boson decays are incorporated in the narrow width approximation. In this approximation, radiative Z decay diagrams, and graphs in which a virtual photon decays into a charged lepton pair can be ignored. Radiative Z decays are of little interest when probing for nonstandard couplings and can be suppressed by a suitable choice of cuts (see Sec. III B). Furthermore, in the narrow width approximation it is particularly easy to extend the NLO calculation of hadronic $Z\gamma$ production in Ref. [11] to include the leptonic decay of the Z boson. The charged leptons are assumed to be massless in our calculation.

A. Summary of $\mathcal{O}(\alpha_s)$ $Z\gamma$ production including leptonic Z decay

At lowest order in the SM, hadronic $Z\gamma$ production proceeds via the Feynman diagrams shown in Fig. 1. Nonstandard $ZZ\gamma$ and $Z\gamma\gamma$ couplings contribute via the graphs shown in Fig. 2. At the leading-logarithm level, there are additional contributions to $Z\gamma$ production which come from photon bremsstrahlung processes such as $qg \rightarrow Zq$ followed by photon bremsstrahlung from the final state quark. Although the process $qg \rightarrow Zq$ is formally of $\mathcal{O}(\alpha\alpha_s)$, the photon fragmentation functions are of order α/α_s [21]; thus the photon bremsstrahlung process is of the same order as the Born process.

The NLO calculation of $Z\gamma$ production includes contributions from the square of the Born graphs, the interference between the Born graphs and the virtual one-loop diagrams, and the square of the real emission graphs. The basic idea of the method employed here is to isolate the soft and collinear singularities associated with the real emission subprocesses by partitioning phase space into soft, collinear, and finite
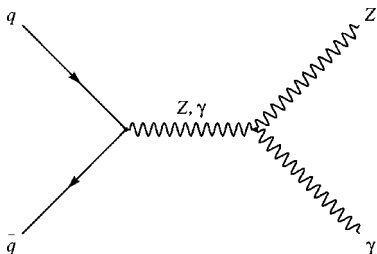

FIG. 2. Additional Feynman diagrams which contribute to the Born level process $q\bar{q} \rightarrow Z\gamma$ when nonstandard model $ZZ\gamma$ and $Z\gamma\gamma$ couplings are introduced.

regions. This is done by introducing theoretical soft and collinear cutoff parameters, δ_s and δ_c. Using dimensional regularization [22], the soft and collinear singularities are exposed as poles in ϵ (the number of space-time dimensions is $N = 4 - 2\epsilon$ with ϵ a small number). The infrared singularities from the soft and virtual contributions are then explicitly canceled while the collinear singularities are factorized and absorbed into the definition of the parton distribution functions. The remaining contributions are finite and can be evaluated in four dimensions. The Monte Carlo program thus generates n-body (for the Born and virtual contributions) and $(n+1)$-body (for the real emission contributions) final state events. The n- and $(n+1)$-body contributions both depend on the cutoff parameters δ_s and δ_c, however, when these contributions are added together to form a suitably inclusive observable, all dependence on the cutoff parameters cancels. The numerical results presented in this paper are insensitive to variations of the cutoff parameters.

Except for the virtual contribution, the $\mathcal{O}(\alpha_s)$ corrections are all proportional to the Born cross section. It is easy to incorporate the leptonic Z decays into those terms which are proportional to the Born cross section; one simply replaces $d\hat{\sigma}^{\text{Born}}(q\bar{q} \rightarrow Z\gamma)$ with $d\hat{\sigma}^{\text{Born}}(q\bar{q} \rightarrow Z\gamma \rightarrow \ell^+\ell^-\gamma)$ or $d\hat{\sigma}^{\text{Born}}(q\bar{q} \rightarrow Z\gamma \rightarrow \bar{\nu}\nu\gamma)$ in the relevant formulas. When working at the amplitude level, the Z boson decay is trivial to implement; the Z boson polarization vector, $\epsilon_\mu(k)$, is simply replaced by the corresponding $Z \rightarrow \ell^+\ell^-$ or $Z \rightarrow \bar{\nu}\nu$ decay current in the amplitude. Details of the amplitude level calculations for the Born and real emission subprocesses can be found in Ref. [23].

The only term in which it is more difficult to incorporate the Z boson decay is the virtual contribution. Rather than undertake the nontrivial task of recalculating the virtual correction term for the case of a leptonically decaying Z boson, we have instead opted to use the virtual correction for a real on-shell Z boson which we subsequently decay ignoring spin correlations. When spin correlations are ignored, the spin summed squared matrix element factorizes into separate production and decay squared matrix elements. Neglecting spin correlations slightly modifies the shapes of the angular distributions of the final state leptons, but does not alter the total cross section as long as no angular cuts (e.g., rapidity cuts) are imposed on the final state leptons. For realistic rapidity cuts, cross sections are changed by typically 10% when spin correlations are neglected. Since the size of the finite virtual correction is only about 2–4% the size of the Born cross section, the overall effect of neglecting the spin correlations in the finite virtual correction is expected to be negligible compared to the combined 10–20% uncertainty from the parton distribution functions, the choice of the factorization scale Q^2, and higher order QCD corrections.

B. General $ZZ\gamma$ and $Z\gamma\gamma$ couplings

In $q\bar{q} \rightarrow Z\gamma$, the timelike virtual photon and/or Z boson couples to essentially massless fermions, which ensures that effectively $\partial_\mu V^\mu = 0$, $V = \gamma, Z$. This fact, together with gauge invariance of the on-shell photon, restricts the tensor structure of the $Z\gamma V$ vertex sufficiently to allow only four free
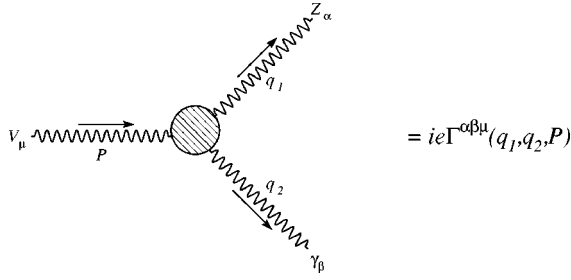
FIG. 3. Feynman rule for the general $Z\gamma V$ ($V = Z, \gamma$) vertex. The factor e is the charge of the proton. The vertex function $\Gamma^{\alpha\beta\mu}_{Z\gamma V}(q_1, q_2, P)$ is given in Eq. (1).

parameters. The most general nonstandard $ZZ\gamma$ vertex function (see Fig. 3 for notation) is [24]

$$
\Gamma^{\alpha\beta\mu}_{Z\gamma Z}(q_1, q_2, P) = \frac{P^2 - q_1^2}{m_Z^2}\Bigg\{ h_1^Z(q_2^\mu g^{\alpha\beta} - q_2^\alpha g^{\mu\beta})
$$
$$
+ \frac{h_2^Z}{m_Z^2} P^\alpha((P \cdot q_2)g^{\mu\beta} - q_2^\mu P^\beta)
$$
$$
+ h_3^Z \epsilon^{\mu\alpha\beta\rho} q_{2\rho} + \frac{h_4^Z}{m_Z^2} P^\alpha \epsilon^{\mu\beta\rho\sigma} P_\rho q_{2\sigma} \Bigg\},
$$

$$(1)$$

where m_Z is the Z boson mass. The most general $Z\gamma\gamma$ vertex function can be obtained from Eq. (1) with the following replacements:

$$
\frac{P^2 - q_1^2}{m_Z^2} \rightarrow \frac{P^2}{m_Z^2} \quad \text{and} \quad h_i^Z \rightarrow h_i^\gamma, \quad i = 1, \ldots, 4. \quad (2)
$$

Terms proportional to P^μ and q_1^α have been omitted in Eq. (1) since they do not contribute to the cross section. Without loss of generality, the overall $ZZ\gamma$ and $Z\gamma\gamma$ coupling has been chosen to be

$$
g_{ZZ\gamma} = g_{Z\gamma\gamma} = e, \quad (3)
$$

where e is the charge of the proton. The overall factor $(P^2 - q_1^2)$ in Eq. (1) is a result of Bose symmetry, whereas the factor P^2 in the $Z\gamma\gamma$ vertex function originates from electromagnetic gauge invariance. As a result, the $Z\gamma\gamma$ vertex function vanishes identically if both photons are on-shell due to Yang's theorem [25].

All the anomalous couplings h_i^V ($i = 1, \ldots, 4$, $V = \gamma, Z$) are C odd; h_1^V and h_2^V violate CP. h_2^V and h_4^V receive contributions only from operators of dimension ≥ 8. Within the standard model, at tree level, all the couplings h_i^V vanish. At the one loop level, only the CP conserving couplings h_3^V and h_4^V are nonzero [26].

For simplicity, the Z boson mass m_Z has been chosen in Eq. (1) as the energy scale in the denominator of the overall factor and the terms proportional to $h_{2,4}^V$. For a different mass scale, M, all subsequent results can be obtained by scaling $h_{1,3}^V$ ($h_{2,4}^V$) by a factor M^2/m_Z^2 (M^4/m_Z^4).

Tree level unitarity restricts the $ZZ\gamma$ and $Z\gamma\gamma$ couplings uniquely to their standard model values at asymptotically

high energies [27]. This implies that the $Z\gamma V$ couplings h_i^V have to be described by form factors $h_i^V(q_1^2, q_2^2, P^2)$ which vanish when q_1^2, q_2^2, or P^2 becomes large. In $Z\gamma$ production $q_2^2 = 0$ and $q_1^2 \approx m_Z^2$ even when finite Z width effects are taken into account. However, large values of $P^2 = \hat{s}$ will be probed in future hadron collider experiments and the $\hat{s}$ dependence has to be included in order to avoid unphysical results that would violate unitarity. A detailed discussion of unitarity and form factors in nonstandard $Z\gamma$ production can be found in Ref. [10]. We will use generalized dipole form factors of the form

$$
h_i^V(m_Z^2, 0, \hat{s}) = \frac{h_{i0}^V}{(1 + \hat{s}/\Lambda_{FF}^2)^n}, \quad (4)
$$

as advocated in Ref. [10]. The subscript 0 denotes the low energy value of the form factor. The mass scale Λ_{FF} is the scale at which novel interactions, like multiple weak boson or resonance production, may appear. Unless stated otherwise, we use $n = 3$ ($n = 4$) for $h_{1,3}^V$ ($h_{2,4}^V$) and $\Lambda_{FF} = 500$ GeV [$\Lambda_{FF} = 3$ TeV] at the Tevatron [LHC].

At present, the most stringent direct bounds on anomalous $Z\gamma V$ couplings come from $Z\gamma$ production at the Tevatron collider, $Z \rightarrow \bar{\nu}\nu\gamma$ decays at LEP1, and $\gamma +$ invisible particles production at the CERN $e^+ e^-$ collider LEP2. From a search performed in the channels $p\bar{p} \rightarrow Z(\rightarrow \ell^+\ell^-)\gamma$ and $p\bar{p} \rightarrow Z(\rightarrow \bar{\nu}\nu)\gamma$, the D0 Collaboration obtains, from run 1a data [5]

$$
|h_{30}^Z| < 0.78 \ \text{(for } h_{40}^Z = 0), \quad |h_{40}^Z| < 0.19 \ \text{(for } h_{30}^Z = 0),
$$

$$(5)$$

and

$$
|h_{30}^\gamma| < 0.81 \ \text{(for } h_{40}^\gamma = 0), \quad |h_{40}^\gamma| < 0.20 \ \text{(for } h_{30}^\gamma = 0),
$$

$$(6)$$

at the 95% confidence level (C.L.). The limits obtained for h_{10}^V and h_{20}^V virtually coincide with those found for h_{30}^V and h_{40}^V, respectively. The L3 Collaboration obtains a slightly better bound on h_{30}^Z [28]. From $e^+ e^- \rightarrow \gamma +$ invisible particles at LEP2, the DELPHI Collaboration finds a preliminary limit of $|h_{30}^\gamma| < 0.5$ [29]. To derive these limits, the experiments assumed a form factor scale of $\Lambda_{FF} = 500$ GeV with $n = 3$ ($n = 4$) for h_3^V (h_4^V).

It is straightforward to include the nonstandard model couplings in the amplitude level calculations. We computed the $q\bar{q} \rightarrow Z\gamma$ virtual correction with the vertex function of Eq. (1) in the 't Hooft-Veltman scheme [22,30] using the computer algebra program FORM [31]. The resulting expression, however, is too lengthy to present here.

Note that the nonstandard $ZZ\gamma$ and $Z\gamma\gamma$ couplings do not destroy the renormalizability of QCD. Thus the infrared singularities from the soft and virtual contributions are explicitly canceled, and the collinear singularities are factorized and absorbed into the definition of the parton distribution functions, exactly as in the standard model case.

The squared matrix element is bilinear in the anomalous couplings. Due to the antisymmetry of $\epsilon^{\mu\alpha\beta\rho}$, all terms pro-

portional to h_3^V, h_4^V, $h_3^V h_i^V$, and $h_4^V h_i^V$ ($i=1,2$) vanish in the LO as well as in the NLO squared matrix elements, after the sum over the fermion helicities and the photon polarizations is performed. Terms proportional to h_1^V and h_2^V are present in the squared matrix elements. These terms are proportional to $\cos \theta^*$, where θ^* is the scattering angle of the photon in the parton center of mass frame. They vanish after the integration over phase space is performed, unless rapidity cuts on the photon which are not symmetric with respect to $\eta=0$ (where η is the pseudorapidity) are chosen.

III. PHENOMENOLOGICAL RESULTS

We now discuss the phenomenological implications of $\mathcal{O}(\alpha_s)$ QCD corrections and general $ZZ\gamma$ and $Z\gamma\gamma$ couplings in $Z\gamma$ production at the Tevatron ($p\bar{p}$ collisions at $\sqrt{s}=1.8$ TeV) and the LHC (pp collisions at $\sqrt{s}=14$ TeV). First, the input parameters, cuts, and the finite energy resolution smearing used to simulate detector response are briefly described. We then discuss in detail the impact of $\mathcal{O}(\alpha_s)$ QCD corrections on the observability of nonstandard $ZZ\gamma$ and $Z\gamma\gamma$ couplings in $Z(\to \ell^+\ell^-)\gamma$ and $Z(\to \bar{\nu}\nu)\gamma$ production at the Tevatron and LHC. As mentioned in the Introduction, we make no attempt to include the contributions from gluon fusion, $gg\to Z\gamma$, which are formally of $\mathcal{O}(\alpha_s^2)$, into our calculation. Gluon fusion contributes less than 0.2% (6%) to the total $Z\gamma$ cross section at the Tevatron (LHC) [15].

A. Input parameters

The numerical results presented here were obtained using the two-loop expression for α_s. The QCD scale Λ_{QCD} is specified for four flavors of quarks by the choice of the parton distribution functions and is adjusted whenever a heavy quark threshold is crossed so that α_s is a continuous function of Q^2. The heavy quark masses were taken to be $m_b=5$ GeV and $m_t=176$ GeV [32,33].

The SM parameters used in the numerical simulations are $m_Z=91.187$ GeV, $m_W=80.22$ GeV, $\alpha(m_W)=1/128$, and $\sin^2\theta_W=1-(m_W/m_Z)^2$. These values are consistent with recent measurements at LEP, SLC, the CERN $p\bar{p}$ collider, and the Tevatron [34]. The soft and collinear cutoff parameters, discussed in Sec. II A, are fixed to $\delta_s=10^{-2}$ and $\delta_c=10^{-3}$. The parton subprocesses have been summed over u, d, s, and c quarks. The Z boson leptonic branching ratio is taken to be $B(Z\to e^+e^-)=0.034$ and the total width of the Z boson is $\Gamma_Z=2.490$ GeV. Except where otherwise stated, a single scale $Q^2=M_{Z\gamma}^2$, where $M_{Z\gamma}$ is the invariant mass of the $Z\gamma$ pair, has been used for the renormalization scale μ^2 and the factorization scale M^2. The NLO numerical results have been calculated in the modified minimal subtraction ($\overline{\text{MS}}$) scheme [35].

In order to get consistent NLO results it is necessary to use parton distribution functions which have been fit to next-to-leading order. The numerical simulations have been performed using the Martin-Roberts-Stirling (MRS) [36] set A distributions ($\Lambda_4=230$ MeV) in the $\overline{\text{MS}}$ scheme. For convenience, the MRS set A distributions have also been used for the LO calculations.

B. Acceptance cuts

The cuts imposed in our numerical simulations are motivated by two factors: (1) the finite acceptance and resolution of the detector, and (2) the need to suppress radiative Z decays which result in the same final state as $Z\gamma$ production but which are of little interest for the study of anomalous couplings in hadronic collisions. The finite acceptance of the detector is simulated by cuts on the four-vectors of the final state particles. This group of cuts includes requirements on the transverse momentum of the photon and charged leptons for $Z(\to \ell^+\ell^-)\gamma$, and on the missing transverse momentum, $\not{p}_T$, resulting from the non-observation of the neutrinos in $Z(\to \bar{\nu}\nu)\gamma$. Also included in this group are cuts on the pseudorapidity, η, of the photon and the charged leptons. In addition, the charged leptons and the photon are also required to be separated in the pseudorapidity-azimuthal-angle plane

$$\Delta R(\ell,\gamma)=[(\Delta\phi_{\ell\gamma})^2+(\Delta\eta_{\ell\gamma})^2]^{1/2}. \tag{7}$$

Since we ignore photon radiation from the final state lepton line in our calculation, it is necessary to impose cuts which will efficiently suppress contributions from these diagrams. In radiative Z decays the lepton-photon separation sharply peaks at small values due to the collinear singularity associated with the diagrams in which the photon is radiated from the final state lepton line. In the following we shall therefore impose a large separation cut of $\Delta R(\ell,\gamma)>0.7$. Contributions from $Z\to \ell^+\ell^-\gamma$ can be further reduced by an invariant mass cut on the $\ell\ell\gamma$ system of $M(\ell\ell\gamma)>100$ GeV.

At leading order, $Z\gamma$ events are produced not only by the Born subprocess $q\bar{q}\to Z\gamma$ but also by the photon bremsstrahlung process which proceeds via subprocesses such as $qg\to Zq$ followed by photon bremsstrahlung from the final state quark. As demonstrated in Ref. [37], the bremsstrahlung process is significant at LHC energies. However, this process does not involve the $Z\gamma V$ vertices and is thus a background in a search for anomalous $ZZ\gamma$ and $Z\gamma\gamma$ couplings. Fortunately, the photon bremsstrahlung events can be suppressed by requiring the photon to be isolated [37]. A photon isolation cut typically requires the sum of the hadronic energy E_{had} in a cone of size R_0 about the direction of the photon to be less than a fraction ϵ_h of the photon energy E_γ, i.e.,

$$\sum_{\Delta R<R_0} E_{\text{had}} < \epsilon_h E_\gamma, \tag{8}$$

with $\Delta R=[(\Delta\phi)^2+(\Delta\eta)^2]^{1/2}$. To suppress the photon bremsstrahlung background, a photon isolation cut with $\epsilon_h=0.15$ and $R_0=0.7$ [38] will be applied in the numerical results presented in this section. For this value of ϵ_h, the photon bremsstrahlung background is less than a few per cent of the Born $Z\gamma$ signal rate. The complete set of cuts for $Z(\to \ell^+\ell^-)\gamma$ is summarized in the following table.

$$Z\gamma \to \ell^+\ell^-\gamma$$

Tevatron	LHC
$p_T(\gamma) > 10$ GeV	$p_T(\gamma) > 100$ GeV
$p_T(\ell) > 15$ GeV	$p_T(\ell) > 20$ GeV
$|\eta(\gamma)| < 3.0$	$|\eta(\gamma)| < 3.0$
$|\eta(\ell)| < 3.5$	$|\eta(\ell)| < 3.0$
$\Delta R(\ell,\gamma) > 0.7$	$\Delta R(\ell,\gamma) > 0.7$
$M(\ell\ell\gamma) > 100$ GeV	$M(\ell\ell\gamma) > 100$ GeV
$\Sigma_{\Delta R < 0.7} E_{had} < 0.15 E_\gamma$	$\Sigma_{\Delta R < 0.7} E_{had} < 0.15 E_\gamma$

Since our calculation is carried out in the narrow width approximation for the Z boson, no explicit cut on the dilepton invariant mass is imposed.

If the Z boson decays into a pair of neutrinos, the experimental signal is $p\bar{p} \to \gamma \not{p}_T$, with the missing transverse momentum, $\not{p}_T$, resulting from the nonobservation of the neutrino pair. For $Z\gamma \to \not{p}_T\gamma$ at the Tevatron we use the same transverse momentum and pseudo-rapidity cuts as the D0 Collaboration in their $Z(\to \bar{\nu}\nu)\gamma$ analysis [9]. The following table summarizes the cuts imposed for both the Tevatron and LHC analysis.

$$Z\gamma \to \not{p}_T \gamma$$

Tevatron	LHC
$p_T(\gamma) > 40$ GeV	$p_T(\gamma) > 100$ GeV
$\not{p}_T > 40$ GeV	$\not{p}_T > 100$ GeV
no jet with $p_T(j) > 15$ GeV	no jet with $p_T(j) > 50$ GeV
and $|\eta(j)| < 2.5$	and $|\eta(j)| < 3$
$|\eta(\gamma)| < 2.5$	$|\eta(\gamma)| < 3.0$

The high $p_T(\gamma)$ and $\not{p}_T$ cuts, when combined with the jet veto, strongly reduce the background from $W \to e\nu$ events where the electron is misidentified as a photon at the Tevatron. These cuts also eliminate backgrounds from γj production with the jet rapidity outside the range covered by the detector and thus "faking" missing transverse momentum, and jj production where one of the jets is misidentified as a photon, while the other disappears through the beam hole. The large $p_T(\gamma)$ and $\not{p}_T$ cuts at LHC energies are chosen to reduce potentially dangerous backgrounds from $Z+1$ jet production, where the jet is misidentified as a photon, and from processes where particles outside the rapidity range covered by the detector contribute to the missing transverse momentum. Present studies [39,40] indicate that these backgrounds are under control for $p_T(\gamma) > 100$ GeV and $\not{p}_T > 100$ GeV.

C. Finite energy resolution effects

Uncertainties in the energy measurements of the charged leptons and photon in the detector are simulated in the calculation by Gaussian smearing of the particle four-momentum vector with standard deviation σ. For distributions which require a jet definition, e.g., the $Z\gamma + 1$ jet exclusive cross section, the jet four-momentum vector is also smeared. The standard deviation σ depends on the particle type and the detector. The numerical results presented here for the Tevatron and LHC center of mass energies were obtained using σ values based on the CDF [41] and ATLAS [40] specifications, respectively. For $Z(\to \bar{\nu}\nu)\gamma$ production at the Tevatron, the photon and $\not{p}_T$ vectors were smeared using the D0 resolutions given in Ref. [9].

D. $\mathcal{O}(\alpha_s)$ corrections and anomalous $ZZ\gamma$ and $Z\gamma\gamma$ couplings in $Z(\to \ell^+\ell^-)\gamma$ production

Nonstandard $ZZ\gamma$ and $Z\gamma\gamma$ couplings have a significant effect on many distributions in $Z\gamma$ production. The photon transverse momentum distribution was found [10] to be the distribution most sensitive to anomalous couplings. We will therefore concentrate on it in the following presentation.

The LO and NLO SM photon transverse momentum distributions for $p\bar{p} \to Z\gamma + X \to \ell^+\ell^-\gamma + X$ production at Tevatron and LHC center of mass energies are shown in Fig. 4. Here, and in all subsequent results shown for $Z \to \ell^+\ell^-$ decays, we sum over electron and muon final states. The NLO corrections grow with the photon transverse momentum and with the center of mass energy. At the LHC, for example, the QCD corrections increase the SM cross section by about a factor 2.2 at $p_T(\gamma) = 1$ TeV, whereas the enhancement is only a factor 1.4 at $p_T(\gamma) = 100$ GeV. The large QCD corrections at high values of $p_T(\gamma)$ are caused by a collinear enhancement factor, $\log^2[p_T(\gamma)/m_Z]$, in the $qg \to Z\gamma q$ partonic cross section for photon transverse momenta much larger than m_Z, $p_T(\gamma) \gg m_Z$, and the large qg luminosity at LHC energies. The large corrections arise from the kinematical region where the photon is produced at large p_T and recoils against the quark, which radiates a soft Z boson which is almost collinear to the quark, and thus is similar in nature to the enhancement of QCD corrections observed at large vector boson transverse momenta in $W\gamma$, WZ, and W^+W^- production [16,18,20]. The effect, however, is less pronounced than in these processes. In $W\gamma$ and WZ production, the SM Born cross section is suppressed due to the appearance of an exact or approximate radiation zero [42,43], while there is no radiation zero in the $Z\gamma$ case. In W^+W^- production, the strong correlation of the W helicities in the SM, together with the effect of kinematic cuts, is responsible for the larger effect of the QCD corrections [19].

The effects of nonstandard $ZZ\gamma$ couplings on the photon transverse momentum distribution in $p\bar{p} \to Z\gamma + X \to \ell^+\ell^-\gamma + X$ at the Tevatron center of mass energy are shown in Fig. 5. The LO and NLO results are shown in

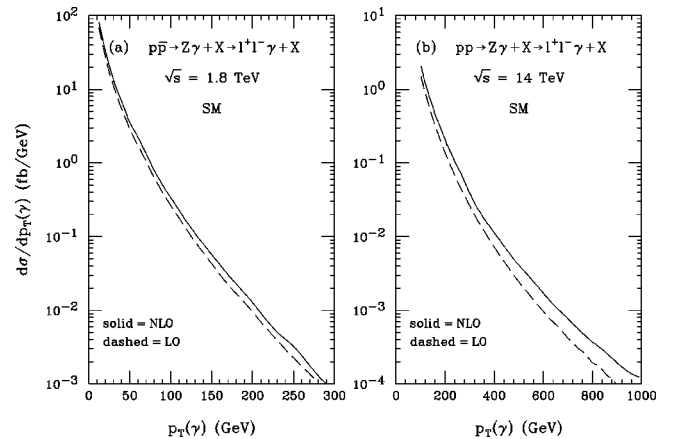FIG. 4. Differential cross sections versus $p_T(\gamma)$ for (a) $p\bar{p} \to Z\gamma + X \to \ell^+\ell^-\gamma + X$ at $\sqrt{s} = 1.8$ TeV, and (b) $pp \to Z\gamma + X \to \ell^+\ell^-\gamma + X$ at $\sqrt{s} = 14$ TeV in the SM. The jet-inclusive cross sections are shown at the Born level (dashed curves) and with the NLO corrections (solid curves). The cuts imposed are summarized in Sec. III B.
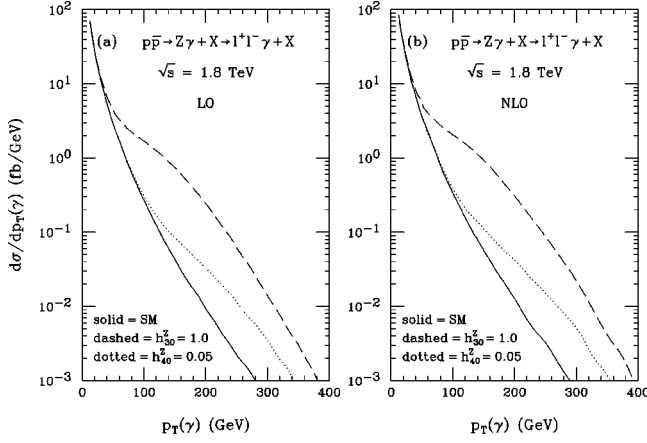
FIG. 5. The differential cross section for the photon transverse momentum in the reaction $p\bar{p}\rightarrow Z\gamma+X\rightarrow\ell^{+}\ell^{-}\gamma+X$ at $\sqrt{s}=1.8$ TeV, (a) in the Born approximation and (b) including NLO QCD corrections. The curves are for the SM (solid), $h_{30}^{Z}=1.0$ (dashed), and $h_{40}^{Z}=0.05$ (dotted). The cuts imposed are summarized in Sec. III B.

FIG. 6. The differential cross section for the photon transverse momentum in the reaction $pp\rightarrow Z\gamma+X\rightarrow\ell^{+}\ell^{-}\gamma+X$ at $\sqrt{s}=14$ TeV, (a) in the Born approximation and (b) including NLO QCD corrections. The curves are for the SM (solid), $h_{30}^{Z}=0.01$ (dashed), and $h_{40}^{Z}=1\times10^{-4}$ (dotted). The cuts imposed are summarized in Sec. III B.

Fig. 5a and Fig. 5b, respectively. Results are displayed for the SM and two sets of anomalous couplings ($h_{30}^{Z}=1.0$, $h_{40}^{Z}=h_{10}^{Z}=h_{20}^{Z}=0$, SM $Z\gamma\gamma$ couplings) and ($h_{40}^{Z}=0.05$, $h_{30}^{Z}=h_{10}^{Z}=h_{20}^{Z}=0$, SM $Z\gamma\gamma$ couplings). For simplicity, only one coupling at a time is allowed to differ from its SM value. In order to clearly display the effect of the anomalous couplings, we have chosen rather large values for h_{30}^{Z} and h_{40}^{Z}, here as well as for the LHC (see below). However, S-matrix unitarity is respected for the chosen values of the anomalous couplings, the power of the form factor, and the form factor scale. The $\mathcal{O}(\alpha_{s})$ corrections in the presence of anomalous couplings at the Tevatron energy are approximately 20–40%, as in the SM.

For equal coupling strengths, the numerical results obtained for the $Z\gamma\gamma$ couplings h_{30}^{γ} and h_{40}^{γ} are about 20% below those obtained for h_{30}^{Z} and h_{40}^{Z} in the region where anomalous coupling effects dominate over the SM cross section. Results for the CP-violating couplings $h_{1,2}^{V}$ ($V=Z,\gamma$) are identical to those obtained for the same values of $h_{3,4}^{V}$. Since terms linear in the anomalous couplings vanish in the differential cross sections, results are insensitive to the sign of the anomalous couplings if only one coupling at a time is allowed to differ from its SM value.

The $p_{T}(\gamma)$ distribution for $Z(\rightarrow\ell^{+}\ell^{-})\gamma$ production at the LHC is shown in Fig. 6. At leading order, the sensitivity of the photon transverse momentum distribution to anomalous $ZZ\gamma$ couplings is significantly more pronounced than at the Tevatron. In the presence of anomalous couplings, the higher order QCD corrections are considerably smaller than in the SM. For large values of $p_{T}(\gamma)$, when anomalous couplings dominate, the $\mathcal{O}(\alpha_{s})$ corrections are typically between 20% and 40%. In the same region, QCD corrections enhance the SM cross section by about a factor 2.2. At next-to-leading order, the sensitivity of the photon transverse momentum spectrum to anomalous couplings thus is somewhat reduced at the LHC. The logarithmic factor causing the cross section enhancement at high values of $p_{T}(\gamma)$ in the SM originates from the collinear region. The Feynman diagrams contributing in this region do not involve the $Z\gamma V$ vertices.
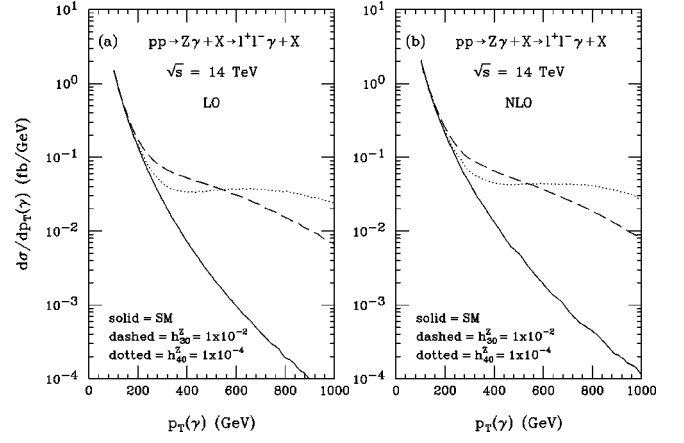
The logarithmic enhancement factor therefore does not affect the anomalous contributions to the matrix elements. Because h_{4}^{Z} receives contributions only from operators with dimension ≥ 8, terms in the helicity amplitudes proportional to it grow like $(\sqrt{s}/m_{Z})^{5}$. Deviations originating from h_{4}^{Z}, therefore, start at higher invariant masses and rise much faster than contributions from couplings such as h_{3}^{Z} which correspond to dimension 6 operators.

The effect of the QCD corrections is shown in more detail in Fig. 7, where we display the ratio of the NLO and LO differential cross sections for the transverse momentum of the photon. At the Tevatron, the NLO to LO cross section ratio slowly rises from 1.2 at $p_{T}(\gamma)=10$ GeV to about 1.5 at $p_{T}(\gamma)=400$ GeV. Since we used a rather small form factor scale of $\Lambda_{FF}=500$ GeV for the Tevatron, the effect of the anomalous couplings is suppressed at high transverse mo-
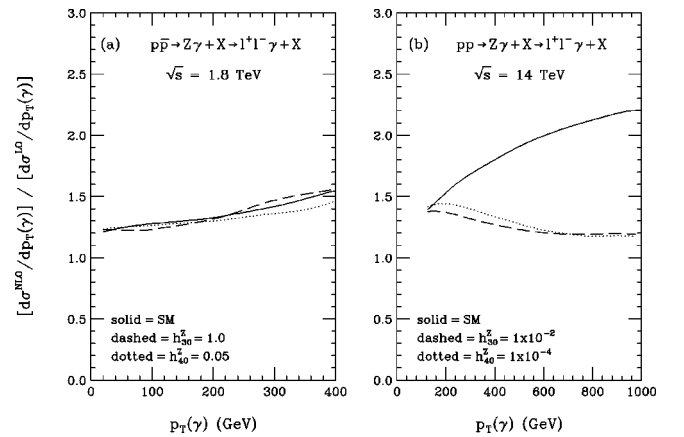

FIG. 7. Ratio of the NLO and LO differential cross sections of the transverse momentum of the photon as a function of $p_{T}(\gamma)$ for (a) $p\bar{p}\rightarrow Z\gamma+X\rightarrow\ell^{+}\ell^{-}\gamma+X$ at $\sqrt{s}=1.8$ TeV, and (b) $pp\rightarrow Z\gamma+X\rightarrow\ell^{+}\ell^{-}\gamma+X$ at $\sqrt{s}=14$ TeV. The solid curves show the SM result. The dashed and dotted lines display the cross section ratio for non-zero values of h_{30}^{Z} and h_{40}^{Z}, respectively. The cuts imposed are summarized in Sec. III B.
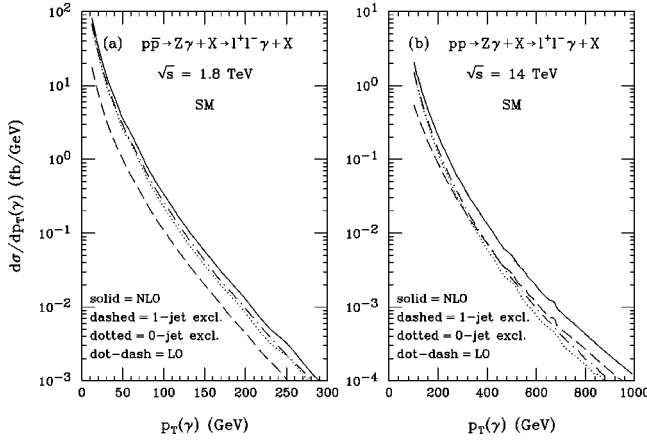
FIG. 8. The $p_T(\gamma)$ differential cross section for (a) $p\bar{p} \to Z\gamma + X \to \ell^+\ell^-\gamma + X$ at $\sqrt{s} = 1.8$ TeV, and (b) $pp \to Z\gamma + X \to \ell^+\ell^-\gamma + X$ at $\sqrt{s} = 14$ TeV in the SM. The inclusive NLO differential cross section (solid line) is decomposed into the $\mathcal{O}(\alpha_s)$ 0-jet (dotted line) and LO 1-jet (dashed line) exclusive differential cross sections. For comparison, the Born cross section (dot dashed line) is also shown. The cuts imposed are summarized in Sec. III B. For the jet definitions, we have used Eqs. (9) and (10).

FIG. 9. The $p_T(\gamma)$ differential cross section for (a) $p\bar{p} \to Z\gamma + 0$ jet $\to \ell^+\ell^-\gamma + 0$ jet at $\sqrt{s} = 1.8$ TeV, and (b) $pp \to Z\gamma + 0$ jet $\to \ell^+\ell^-\gamma + 0$ jet at $\sqrt{s} = 14$ TeV. The curves in part (a) are for the SM (solid), $h_{30}^Z = 1.0$ (dashed), and $h_{40}^Z = 0.05$ (dotted). In part (b), the dashed and dotted curves are for $h_{30}^Z = 10^{-2}$ and $h_{40}^Z = 10^{-4}$, respectively. The cuts imposed are summarized in Sec. III B. For the jet definitions, we have used Eqs. (9) and (10).

menta. As a result, the NLO to LO cross section ratio for non-vanishing anomalous couplings is very similar to that obtained in the SM. At the LHC, we use $\Lambda_{FF} = 3$ TeV and the cross section ratio gradually decreases with $p_T(\gamma)$ from ≈ 1.35 to 1.2 if anomalous couplings are present. In contrast, the SM NLO to LO cross section ratio increases from ≈ 1.35 at $p_T(\gamma) = 100$ GeV to 2.2 at $p_T(\gamma) = 1$ TeV.

From the picture outlined above, one expects that, at next-to-leading order, a large fraction of the $Z\gamma$ events with large photon transverse momentum will contain a high p_T jet at the LHC. At the Tevatron, on the other hand, the jet activity of $Z\gamma$ events at high $p_T(\gamma)$ should be substantially reduced. This fact is illustrated in Fig. 8 which shows the decomposition of the inclusive SM NLO $p_T(\gamma)$ differential cross section into NLO 0-jet and LO 1-jet exclusive cross sections [12]. For comparison, the photon transverse momentum distribution in the Born approximation is also shown in the figure. Here, a jet is defined as a quark or gluon with

$$p_T(j) > 10 \text{ GeV} \quad \text{and} \quad |\eta(j)| < 2.5 \qquad (9)$$

at the Tevatron, and

$$p_T(j) > 50 \text{ GeV} \quad \text{and} \quad |\eta(j)| < 3 \qquad (10)$$

at the LHC. The sum of the NLO 0-jet and the LO 1-jet exclusive cross section is equal to the inclusive NLO cross section. The NLO exclusive $Z\gamma + 0$ jet and the LO exclusive $Z\gamma + 1$ jet cross sections depend explicitly on the jet definition, however, the inclusive NLO cross section is independent of the jet definition.

Present LHC studies [39,40,44] and projections to Tevatron energies suggest that jets fulfilling the criteria of Eqs. (9) and (10) can be identified in $Z\gamma + X$ events at the Tevatron [45] and LHC [46] for luminosities up to 10^{33} cm^{-2} s^{-1} and 10^{34} cm^{-2} s^{-1}, respectively. It should be noted, however, that for theoretical reasons, the jet transverse momen-
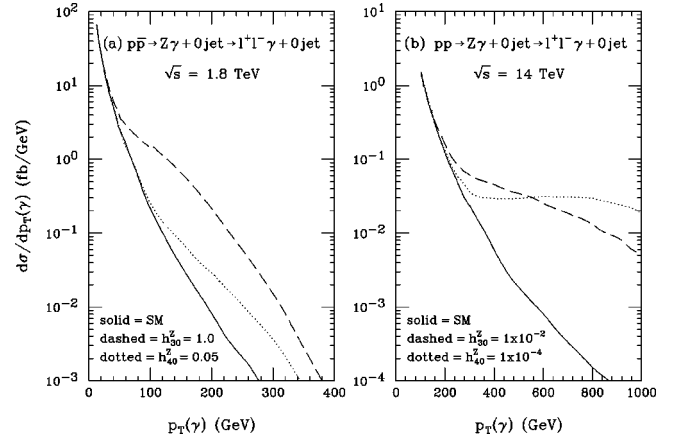
tum threshold cannot be made arbitrarily small in our calculation. For transverse momenta below 5 GeV (20 GeV) at the Tevatron (LHC), soft gluon resummation effects are expected to significantly change the shape of the jet p_T distribution [47]. For the jet definitions discussed above, these effects are expected to be unimportant and therefore are ignored in our calculation.

Figure 8 shows that, at the Tevatron, the 1-jet cross section is always considerably smaller than the NLO 0-jet rate. At the LHC, on the other hand, the 1-jet cross section is larger than the LO cross section for $p_T(\gamma) > 400$ GeV. The effect of the QCD corrections can be reduced by vetoing hard jets in the central rapidity region, i.e., by imposing a ``zero jet'' requirement and considering $Z\gamma + 0$ jet production only. The NLO 0-jet and Born differential cross sections deviate by 30% at most in the p_T region shown. The photon transverse momentum distribution for NLO $Z\gamma + 0$ jet production is shown in Fig. 9. The 0-jet requirement is seen to restore the sensitivity to anomalous couplings lost in the inclusive NLO cross section at the LHC. It has little effect at the Tevatron.

As mentioned in Sec. III A, all our results are obtained for a scale of $Q^2 = M_{Z\gamma}^2$. The Born cross section for $Z\gamma$ production depends significantly on the choice of Q, which enters through the scale-dependence of the parton distribution functions. At the NLO level, the Q-dependence enters not only via the parton distribution functions, but also through the running coupling $\alpha_s(Q^2)$ and the explicit factorization scale-dependence in the order $\alpha_s(Q^2)$ correction terms. Similar to the situation encountered in $W\gamma$, WZ, and W^+W^- production in hadronic collisions [16,17,19], we find that the NLO $Z\gamma + 0$ jet exclusive cross section is almost independent of the scale Q. Here, the scale-dependence of the parton distribution functions is compensated by that of $\alpha_s(Q^2)$ and the explicit factorization scale dependence in the correction terms. The Q-dependence of the inclusive NLO cross section is larger than that of the NLO 0-jet cross section; it is dominated by the 1-jet exclusive component which is calculated
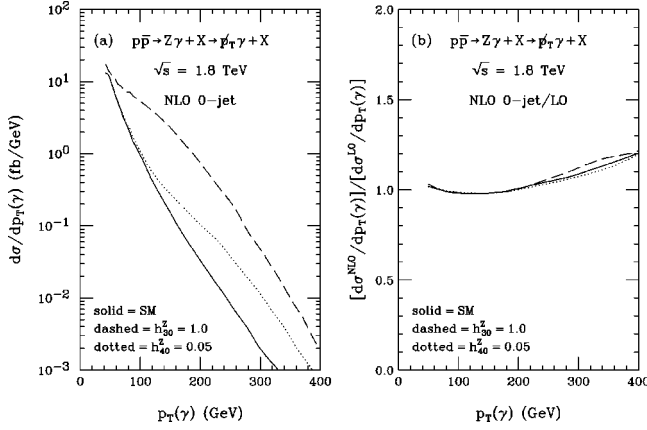
FIG. 10. (a) The $p_T(\gamma)$ differential cross section, and (b) the ratio of the NLO 0-jet to LO differential cross sections of the photon transverse momentum as a function of $p_T(\gamma)$ for $p\bar{p} \rightarrow Z\gamma + 0$ jet$\rightarrow \not{p}_T\gamma + 0$ jet at $\sqrt{s} = 1.8$ TeV. The curves are for the SM (solid), $h_{30}^Z = 1.0$ (dashed), and $h_{40}^Z = 0.05$ (dotted). The cuts imposed are summarized in Sec. III B.
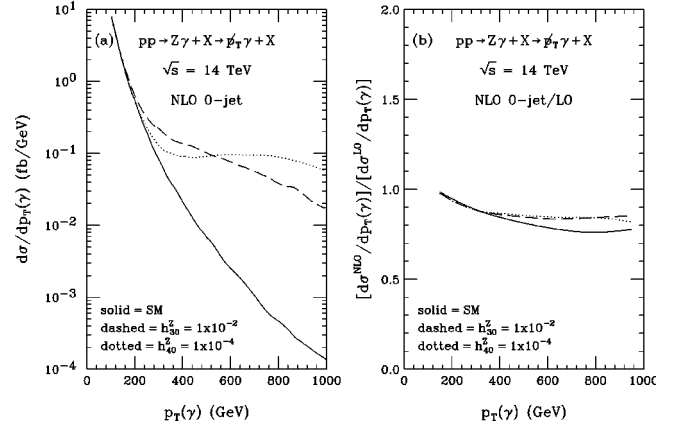
FIG. 11. (a) The $p_T(\gamma)$ differential cross section, and (b) the ratio of the NLO 0-jet to LO differential cross sections of the photon transverse momentum as a function of $p_T(\gamma)$ for $pp \rightarrow Z\gamma + 0$ jet$\rightarrow \not{p}_T\gamma + 0$ jet at $\sqrt{s} = 14$ TeV. The curves are for the SM (solid), $h_{30}^Z = 10^{-2}$ (dashed), and $h_{40}^Z = 10^{-4}$ (dotted). The cuts imposed are summarized in Sec. III B.

only to lowest order and thus exhibits a considerable scale-dependence.

E. $\mathcal{O}(\alpha_s)$ corrections and anomalous $ZZ\gamma$ and $Z\gamma\gamma$ couplings in $Z(\rightarrow \bar{\nu}\nu)\gamma$ production

If the Z boson produced in $q\bar{q} \rightarrow Z\gamma$ decays into neutrinos, the signal consists of a high p_T photon accompanied by a large amount of missing transverse momentum, $\not{p}_T$. Due to the larger $Z \rightarrow \bar{\nu}\nu$ branching ratio, the $\gamma\not{p}_T + X$ differential cross section is about a factor 3 larger than that for $q\bar{q} \rightarrow e^+e^-\gamma + X$ and $q\bar{q} \rightarrow \mu^+\mu^-\gamma + X$ combined. This results in limits on the anomalous $ZZ\gamma$ and $Z\gamma\gamma$ couplings which are presently about a factor 2 better than those obtained from the $Z(\rightarrow \ell^+\ell^-)\gamma$ analysis [9].

The NLO photon transverse momentum distribution for $Z(\rightarrow \bar{\nu}\nu)\gamma$ production at the Tevatron is shown in Fig. 10a. Here we have imposed the cuts of the D0 $Z(\rightarrow \bar{\nu}\nu)\gamma$ analysis (see Sec. III B and Ref. [9]). Since jets with a transverse energy larger than 15 GeV are excluded in the experimental analysis, only the 0-jet differential cross section is shown. The effect of nonstandard $Z\gamma V$ couplings is very similar to that observed in $Z(\rightarrow \ell^+\ell^-)\gamma$ production. The impact of the QCD corrections on the differential cross section is shown in Fig. 10b, where we display the ratio of the NLO and LO differential cross sections for the transverse momentum of the photon. Because of the jet veto cut imposed, the QCD corrections are small over a wide range of photon transverse momenta. For $p_T(\gamma) < 200$ GeV, the cross section ratio is almost constant. It rises slowly for larger values of $p_T(\gamma)$. The NLO to LO cross section ratio in the SM and in the presence of anomalous couplings are very similar.

Figure 10b demonstrates that, for data samples containing only a few $Z(\rightarrow \bar{\nu}\nu)\gamma$ events with $p_T(\gamma) > 200$ GeV and for the jet veto cut used, the LO calculation is an adequate approximation. However, increasing or decreasing the jet transverse momentum threshold will change the size of the QCD corrections, and thus increase the deviation of the NLO cal-

culation from the LO result. The calculation of Ref. [10], where the effect of the NLO QCD corrections is approximated by a constant k-factor of $k = 1 + 8\pi\alpha_s/9 \approx 1.34$, overestimates the cross section by about 30% over a wide range of photon transverse momenta. This calculation, together with a jet veto efficiency of 0.84, has been used in the D0 analysis [9] to compare data with the SM prediction, and to extract limits for the $ZZ\gamma$ and $Z\gamma\gamma$ couplings. This procedure overestimates the cross section by about 13%, and the limits obtained are thus slightly better than those extracted using the full NLO calculation (see Sec. III F).

In Fig. 11a we show the NLO photon transverse momentum distribution for $Z(\rightarrow \bar{\nu}\nu)\gamma$ production at the LHC, imposing a $p_T(j) < 50$ GeV jet veto cut. Figure 11b displays the ratio of the NLO and LO differential cross sections for the transverse momentum of the photon. For the $p_T(j)$ threshold chosen, NLO QCD corrections reduce the cross section by up to 20%. In contrast to the situation encountered at the Tevatron, the cross section ratio slowly falls with $p_T(\gamma)$.

F. Sensitivity limits

We now study the impact that $\mathcal{O}(\alpha_s)$ QCD corrections to $Z\gamma$ production have on the sensitivity limits for h_{i0}^V at the Tevatron and LHC. For the Tevatron we consider integrated luminosities of 1 fb^{-1}, as envisioned for the Main Injector era, and 10 fb^{-1} (TeV33) which could be achieved through additional upgrades of the Tevatron accelerator complex [45]. In the case of the LHC we use $\int \mathcal{L}dt = 10$ fb^{-1} and 100 fb^{-1} [46]. To extract limits in the $Z(\rightarrow \ell^+\ell^-)\gamma$ case, we sum over electron and muon final states. Interference effects between different $Z\gamma V$ ($V = Z, \gamma$) couplings are fully incorporated in our analysis.

To derive 95% C.L. limits we use the $p_T(\gamma)$ distribution and perform a χ^2 test [10], assuming that no deviations from the SM predictions are observed in the experiments considered. We include the cuts summarized in Sec. III B. For $Z(\rightarrow \ell^+\ell^-)\gamma$ production, we use the jet definitions of Eqs. (9) and (10). Unless explicitly stated otherwise, a form factor as given in Eq. (4) is used with $n = 3$ for $h_{1,3}^V$, and $n = 4$ for
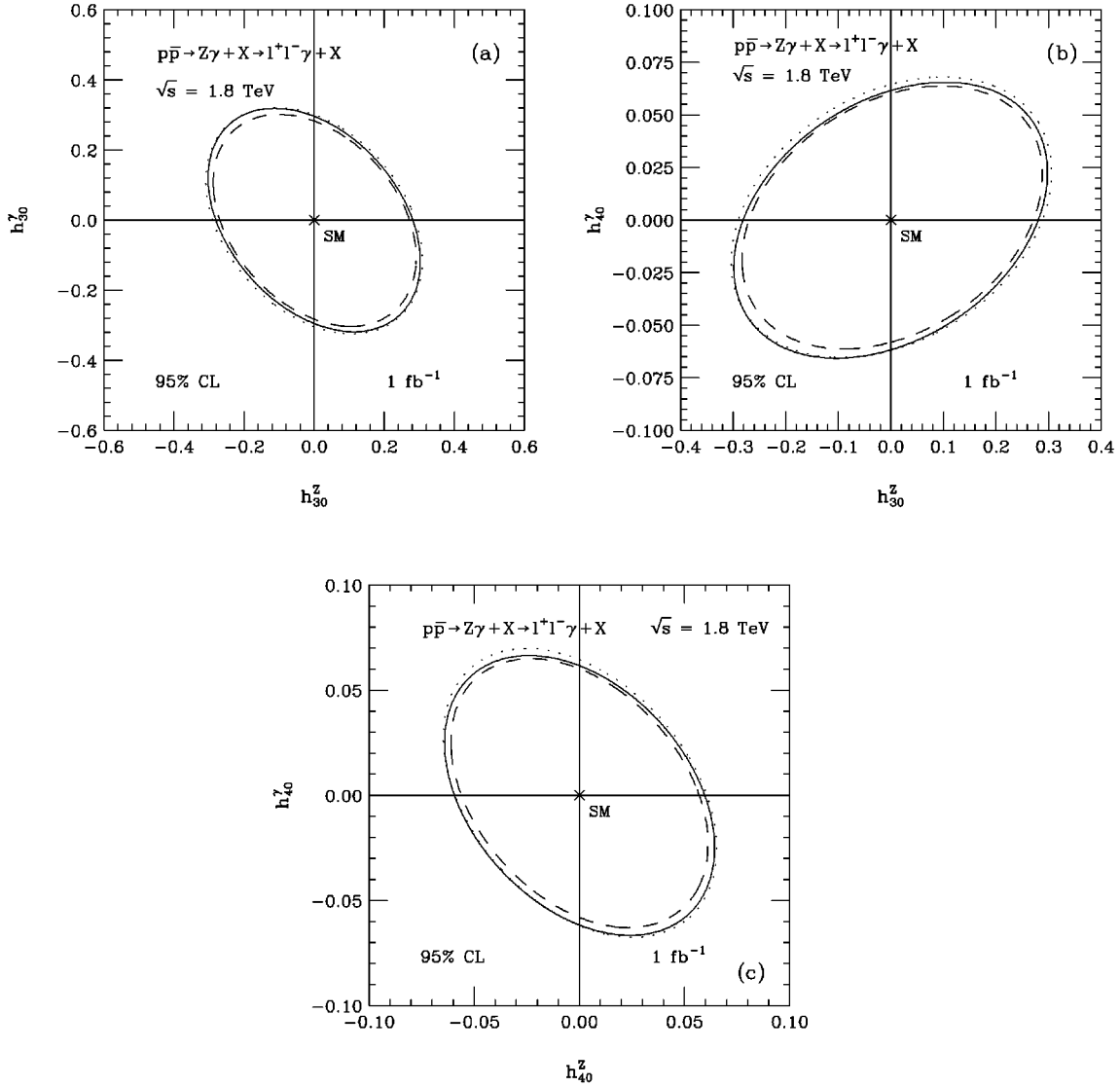
FIG. 12. Limit contours at the 95% C.L. for $p\bar{p} \to Z\gamma + X \to \ell^+\ell^-\gamma + X$ ($\ell = e, \mu$), derived from the $p_T(\gamma)$ distribution at the Tevatron for $\int \mathcal{L}dt = 1$ fb^{-1}. Contours are shown in three planes: (a) the $h_{30}^Z - h_{30}^\gamma$ plane, (b) the $h_{30}^Z - h_{40}^\gamma$ plane, and (c) the $h_{40}^Z - h_{40}^\gamma$ plane. The solid lines give the results for LO $Z\gamma$ production. The dashed curves give the inclusive NLO results, and the dotted lines show the bounds obtained from the exclusive $Z\gamma + 0$ jet channel. In each graph, only those couplings which are plotted against each other are assumed to be different from their zero SM values. The cuts imposed are summarized in Sec. III B. For the jet definition, we have used Eq. (9).

$h_{2,4}^V$. Furthermore, the form factor scale Λ_{FF} is taken to be 0.5 TeV (3.0 TeV) for Tevatron (LHC) simulations. The $p_T(\gamma)$ distribution is split into a certain number of bins. The number of bins and the bin width depend on the center of mass energy and the integrated luminosity. In each bin the Poisson statistics are approximated by a Gaussian distribution. In order to achieve a sizable counting rate in each bin, all events above a certain threshold are collected in a single bin. This procedure guarantees that a high statistical significance cannot arise from a single event at large transverse momentum, where the SM predicts much less than one event. In order to derive realistic limits we allow for a normalization uncertainty of 50% in the SM cross section. For the cuts we impose, background contributions other than SM $Z\gamma$ production are small [10] and are ignored in our derivation of sensitivity limits.

The calculation of sensitivity bounds is facilitated by the observation that the CP conserving couplings $h_{3,4}^V$ and the CP violating couplings $h_{1,2}^V$ do not interfere. Furthermore, cross sections and sensitivities are nearly identical for equal values of $h_{10,20}^V$ and $h_{30,40}^V$. In the following we shall therefore concentrate on $h_{3,4}^V$. In each bin, i, the cross section is a bilinear function of the anomalous couplings:

$$\sigma^i = \sigma^i(SM) + \sum_{V=\gamma,Z} (a_3^{iV}h_3^V + a_4^{iV}h_4^V)$$

$$+ \sum_{V,V'=\gamma,Z} \sum_{j,k=3,4} b_{jk}^{iVV'}h_j^V h_k^{V'} . \qquad (11)$$

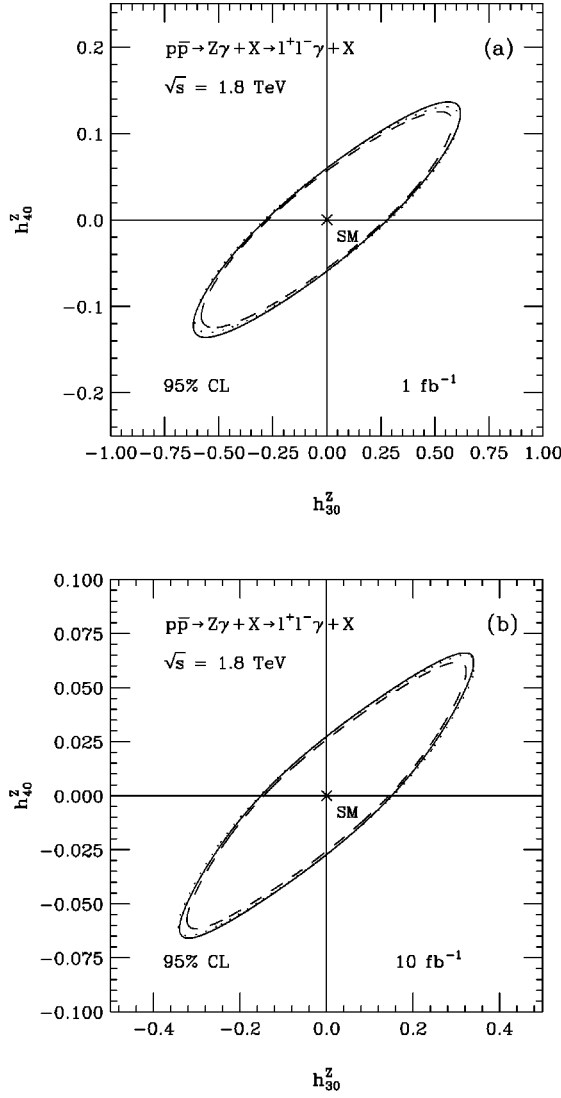Here, $\sigma^i(SM)$ is the SM cross section, and $a_{3,4}^{iV}$ and $b_{jk}^{iVV'}$ are

FIG. 13. Limit contours at the 95% C.L. in the $h_{30}^Z - h_{40}^Z$ plane for $p\bar{p} \to Z\gamma + X \to \ell^+ \ell^- \gamma + X$ ($\ell = e, \mu$), derived from the $p_T(\gamma)$ distribution at the Tevatron for (a) $\int \mathcal{L} dt = 1$ fb^{-1} and (b) $\int \mathcal{L} dt = 10$ fb^{-1}. The solid lines give the results for LO $Z\gamma$ production. The dashed curves give the inclusive NLO results, and the dotted lines show the bounds obtained from the exclusive $Z\gamma + 0$ jet channel. $h_{1,2}^Z$ and all $Z\gamma\gamma$ couplings are assumed to be zero. The cuts imposed are summarized in Sec. III B. For the jet definition, we have used Eq. (9).

constants. Since the interference terms between the SM and the anomalous contributions to the helicity amplitudes vanish for $h_{3,4}^V$ (see Sec. II B),

$$a_3^{iV} = a_4^{iV} = 0. \tag{12}$$

These constraints are taken into account in our calculation of sensitivity bounds.

For $h_{1,2}^V$, an expression for the cross section similar to that of Eq. (11) can be derived. In this case, however, the coefficients of the terms linear in $h_{1,2}^V$ only vanish if the phase space integration over the scattering angle of the photon, θ, is symmetric in $\cos \theta$ (see Sec. II B).

Our results are summarized in Figs. 12–15 and Tables

I–III. Figure 12 shows 95% C.L. contours in the $h_{30}^Z - h_{30}^\gamma$, $h_{30}^Z - h_{40}^\gamma$, and the $h_{40}^Z - h_{40}^\gamma$ plane for $Z(\to \ell^+ \ell^-)\gamma$ production and an integrated luminosity of 1 fb^{-1} at the Tevatron. Results for the $h_{30}^\gamma - h_{40}^Z$ plane are very similar to those displayed in Fig. 12b for h_{30}^Z versus h_{40}^γ, and are therefore not shown. In each figure, only those couplings which are plotted against each other are assumed to be different from their zero SM values. As noted in Ref. [10], $ZZ\gamma$ and $Z\gamma\gamma$ couplings interfere little at LO. Figure 12 demonstrates that the NLO QCD corrections do not change this behavior. This statement also applies to different integrated luminosities and to $Z(\to \ell^+ \ell^-)\gamma$ production at the LHC. Due to the larger cross section, the sensitivity bounds obtained from the inclusive NLO differential cross section are about 5% better than those derived using the LO calculation. The limits extracted from the NLO $Z\gamma + 0$ jet cross section are almost identical to those found using the LO calculation.

Larger correlations are encountered between h_3^V and h_4^V (see Ref. [10]). The impact of the $\mathcal{O}(\alpha_s)$ QCD corrections on the limits in the $h_3^Z - h_4^Z$ plane at the Tevatron is shown in Fig. 13 for integrated luminosities of 1 fb^{-1} and 10 fb^{-1}. The inclusive NLO QCD corrections improve the sensitivity bounds by up to 9% (6%) for 1 fb^{-1} (10 fb^{-1}) whereas the limits obtained analyzing the $Z\gamma + 0$ jet channel are very similar to those found using the LO calculation. Similar results are obtained for h_3^γ and h_4^γ. The sensitivity bounds for the $Z\gamma\gamma$ couplings are a few percent weaker than those found for the corresponding $ZZ\gamma$ couplings, and QCD corrections have a smaller effect than in the case of the $ZZ\gamma$ couplings. Table I summarizes the 95% C.L. sensitivity limits, including all correlations, at leading order and next-to-leading order for h_{30}^V and h_{40}^V ($V = Z, \gamma$) for the process $p\bar{p} \to Z\gamma + X \to \ell^+ \ell^- \gamma + X$ at the Tevatron with $\int \mathcal{L} dt = 1$ fb^{-1}.

Figure 14 displays how the 95% C.L. contour limits for $p\bar{p} \to Z\gamma + X \to \not{p}_T \gamma + X$ at the Tevatron and an integrated luminosity of 1 fb^{-1} are affected by NLO QCD corrections. Since a jet veto cut of $p_T(j) < 15$ GeV is imposed, we only show the LO (solid line) and NLO 0-jet (dotted line) contour limits. As we have demonstrated in Sec. III E, the NLO QCD corrections to $Z(\to \bar{\nu}\nu)\gamma$ production at the Tevatron are small over a large range of photon transverse momenta due

TABLE I. Sensitivities achievable at the 95% confidence level for the anomalous $Z\gamma V$ couplings h_{30}^V and h_{40}^V ($V = Z, \gamma$) in $p\bar{p} \to Z\gamma + X \to \ell^+ \ell^- \gamma + X$, $\ell = e, \mu$, at the Tevatron ($\sqrt{s} = 1.8$ TeV) with $\int \mathcal{L} dt = 1$ fb^{-1}. The limits for each coupling apply for arbitrary values of the other couplings listed in this table. The CP violating couplings $h_{1,2}^V$ are assumed to take their SM values. For the form factor we use the form of Eq. (4) with $n = 3$ ($n = 4$) for h_3^V (h_4^V) and $\Lambda_{FF} = 0.5$ TeV. The cuts summarized in Sec. III B are imposed. For the jet definition, we have used Eq. (9).

Coupling	LO	NLO incl.	NLO 0-jet
$|h_{30}^Z|$	0.62	0.58	0.61
$|h_{40}^Z|$	0.136	0.124	0.130
$|h_{30}^\gamma|$	0.65	0.64	0.68
$|h_{40}^\gamma|$	0.141	0.138	0.148

TABLE II. Sensitivities achievable at the 95% confidence level for the anomalous $ZZ\gamma$ couplings h_{30}^Z and h_{40}^Z in $p\bar{p} \to Z\gamma + X \to \not{p}_T \gamma + X$ at the Tevatron ($\sqrt{s} = 1.8$ TeV) for (a) $\int \mathcal{L} dt = 1$ fb^{-1}, and (b) $\int \mathcal{L} dt = 10$ fb^{-1}. Shown are the limits obtained from the LO calculation, the full NLO 0-jet differential cross section, and the calculation of Ref. [10] using an effective k factor of $k_{\text{eff}} = 1.13$. The limits for each coupling apply for arbitrary values of the other coupling listed in this table. The CP violating couplings $h_{1,2}^Z$ and all $Z\gamma\gamma$ couplings are assumed to vanish. For the form factor we use the form of Eq. (4) with $n = 3$ ($n = 4$) for h_3^Z (h_4^Z) and $\Lambda_{FF} = 0.5$ TeV. The cuts summarized in Sec. III B are imposed. For the jet definition, we have used Eq. (9).

	(a) $\int \mathcal{L} dt = 1$ fb^{-1}		
Coupling	LO	NLO 0-jet	NLO appr.
$|h_{30}^Z|$	0.55	0.53	0.50
$|h_{40}^Z|$	0.108	0.104	0.099
	(b) $\int \mathcal{L} dt = 10$ fb^{-1}		
Coupling	LO	NLO 0-jet	NLO appr.
$|h_{30}^Z|$	0.30	0.29	0.28
$|h_{40}^Z|$	0.055	0.053	0.051

to the 0-jet requirement. The sensitivities achievable for h_{30}^Z and h_{40}^Z in $p\bar{p} \to Z\gamma + X \to \not{p}_T \gamma + X$ at the Tevatron for $\int \mathcal{L} dt = 1$ fb^{-1} and $\int \mathcal{L} dt = 10$ fb^{-1} are listed in Table II. Besides the LO and NLO 0-jet bounds, we also show the limits obtained using the calculation of Ref. [10] with the NLO corrections approximated by a constant effective k-factor $k_{\text{eff}} = 0.84$ $(1 + 8\pi\alpha_s/9) \approx 1.13$. This calculation has been used to extract bounds on $Z\gamma V$ couplings from $Z(\to \bar{\nu}\nu)\gamma$ production at the Tevatron [9]. Since a constant k-factor overestimates the cross section for the jet veto cut imposed in the current experimental analysis of the $Z(\to \bar{\nu}\nu)\gamma$ channel, the sensitivity limits obtained are 4–6% better than those found using the full NLO 0-jet calculation, depending on the integrated luminosity. Results similar to those shown in Fig. 14 and Table II are obtained for $h_{3,4}^\gamma$.

The 95% C.L. limit contours in the h_{30}^Z–h_{40}^Z plane for $Z(\to \ell^+\ell^-)\gamma$ production at the LHC are shown in Fig. 15, assuming an integrated luminosity of 100 fb^{-1}. Table III summarizes the LO and NLO sensitivity bounds for $pp \to Z\gamma + X \to \ell^+\ell^-\gamma + X$ and $pp \to Z\gamma + X \to \not{p}_T \gamma + X$ at $\sqrt{s} = 14$ TeV with $\int \mathcal{L} dt = 10$ fb^{-1} and 100 fb^{-1}. At LHC energies, the inclusive $\mathcal{O}(\alpha_s)$ QCD corrections in the SM considerably change the shape of the $p_T(\gamma)$ distribution (see Fig. 8b). As a result, the inclusive NLO QCD corrections reduce the sensitivity to anomalous couplings by 7–10%. As the integrated luminosity increases, larger transverse momenta become accessible. The difference between the LO and NLO sensitivity bounds for 100 fb^{-1} therefore is slightly larger than for 10 fb^{-1}. In Sec. III D we have demonstrated that the size of the $\mathcal{O}(\alpha_s)$ QCD corrections at the LHC in the high $p_T(\gamma)$ region can be reduced by vetoing hard jets in the central rapidity region. The sensitivity bounds obtained for the $Z\gamma + 0$ jet channel are about 5% better than those found for the inclusive NLO case. However, because the NLO 0-jet cross section is smaller than the LO cross section for the jet
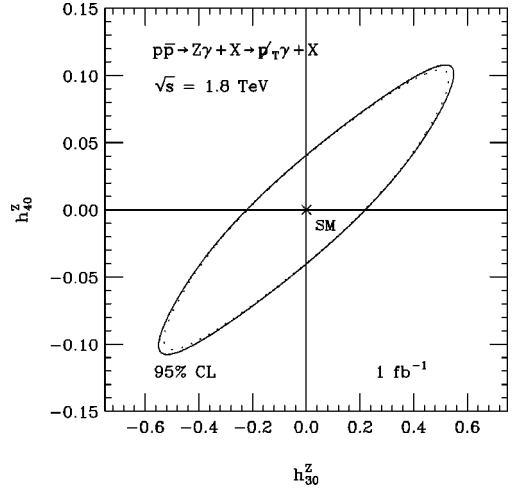

FIG. 14. Limit contours at the 95% C.L. in the h_{30}^Z–h_{40}^Z plane for $p\bar{p} \to Z\gamma + X \to \not{p}_T \gamma + X$ derived from the $p_T(\gamma)$ distribution at the Tevatron for $\int \mathcal{L} dt = 1$ fb^{-1}. The solid line gives the result for LO $Z\gamma$ production. The dotted curve shows the bounds obtained from the NLO calculation. $h_{1,2}^Z$ and all $Z\gamma\gamma$ couplings are assumed to be zero. The cuts imposed are summarized in Sec. III B.

definition we use (see Fig. 8b), the limits obtained in the NLO $Z\gamma + 0$ jet case are slightly worse than those extracted from the LO cross section.

As we have mentioned in Sec. III D, the NLO $Z\gamma + 0$ jet differential cross section is more stable to variations of the factorization scale Q^2 than the LO and inclusive NLO $Z\gamma + X$ cross sections. The systematic errors which originate from the choice of Q^2 will thus be smaller for bounds derived from the NLO $Z\gamma + 0$ jet than those obtained from the inclusive NLO $Z\gamma + X$ or the LO cross section.

As discussed in Ref. [10], the limits which can be achieved are sensitive to the form and the scale of the form
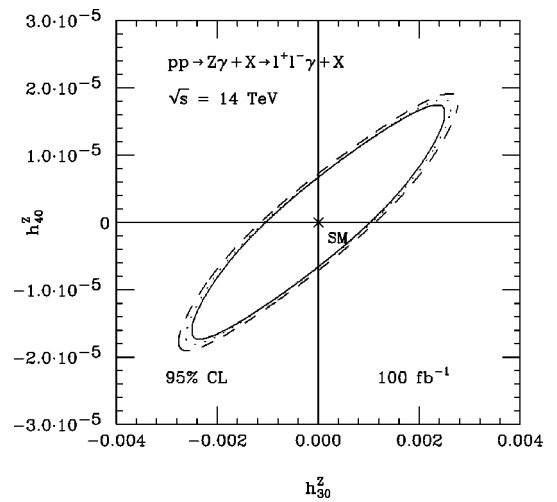

FIG. 15. Limit contours at the 95% C.L. in the h_{30}^Z–h_{40}^Z plane for $pp \to Z\gamma + X \to \ell^+\ell^-\gamma + X$ ($\ell = e, \mu$) derived from the $p_T(\gamma)$ distribution at the LHC for $\int \mathcal{L} dt = 100$ fb^{-1}. The solid line gives the results for LO $Z\gamma$ production. The dashed curve gives the inclusive NLO results, and the dotted lines shows the bounds obtained from the exclusive $Z\gamma + 0$ jet channel. $h_{1,2}^Z$ and all $Z\gamma\gamma$ couplings are assumed to be zero. The cuts imposed are summarized in Sec. III B. For the jet definition, we have used Eq. (10).

factor. For example, doubling the form factor scale to $\Lambda_{FF}=1$ TeV at the Tevatron improves the bounds by almost a factor 3. The dependence of the limits on Λ_{FF} can be understood easily from Figs. 5 and 6. The improvement in sensitivity with increasing Λ_{FF} is due to the additional events at large $p_T(\gamma)$ which are suppressed by the form factor if the scale Λ_{FF} has a smaller value. To a lesser degree, the bounds also depend on the power n in the form factor. Reducing n allows for additional high $p_T(\gamma)$ events and therefore leads to a somewhat increased sensitivity to the low energy values of the anomalous couplings. It should be noted, however, that n must be larger than 3/2 (5/2) for $h_{1,3}^V$ ($h_{2,4}^V$) in order to preserve S-matrix unitarity [10].

The bounds derived in this section are quite conservative. Using more powerful statistical tools than the simple χ^2 test we performed can lead to considerably improved limits [48]. The effect of the NLO QCD corrections on the sensitivity bounds, however, does not depend on the technique used to extract them.

IV. SUMMARY

Hadronic $Z\gamma$ production can be used to probe for non-standard self interactions of the photon and Z boson. The experimental limits for nonstandard $ZZ\gamma$ and $Z\gamma\gamma$ couplings [5,7–9] so far have been based on leading order calculations [10]. In this paper we have presented an $\mathcal{O}(\alpha_s)$ calculation of the reactions $p\overset{(-)}{p}\to Z\gamma+X\to\ell^+\ell^-\gamma+X$ and $p\overset{(-)}{p}\to Z\gamma+X\to\not p_T\gamma+X$ for general $ZZ\gamma$ and $Z\gamma\gamma$ couplings. The leptonic decay of the Z boson has been included in the narrow width approximation in our calculation. Decay spin correlations are correctly taken into account, except in the finite virtual contribution. The finite virtual correction term contributes only at the few per cent level to the total NLO cross section, thus decay spin correlations can be safely ignored here. Photon radiation from the final state lepton line is not taken into account; effects from $Z\to\ell^+\ell^-\gamma$ decays can easily be suppressed by imposing a $\ell\ell\gamma$ invariant mass cut and a cut on the lepton photon separation.

The $p_T(\gamma)$ differential cross section is very sensitive to nonstandard $Z\gamma V$ ($V=Z,\gamma$) couplings. QCD corrections change the shape of this distribution. The shape change is due to a logarithmic enhancement factor in the qg and $\bar q g$ real emission subprocesses which appears in the high $p_T(\gamma)$ region of phase space where the photon is balanced by a high p_T quark which radiates a soft Z boson. The logarithmic enhancement factor combined with the large gluon density at high center of mass energies make the $\mathcal{O}(\alpha_s)$ corrections quite large for $p_T(\gamma)\gg m_Z$. Since the Feynman diagrams responsible for the enhancement at large $p_T(\gamma)$ do not involve any $Z\gamma V$ couplings, inclusive $\mathcal{O}(\alpha_s)$ QCD corrections to $Z\gamma$ production tend to reduce the sensitivity to anomalous couplings.

At the Tevatron, $Z\gamma$ production proceeds mainly via $q\bar q$ annihilation. Here the main effect of the QCD corrections is an increase of the cross section by about 20–25%. The sensitivity limits derived from the inclusive NLO $Z\gamma+X$ cross section at the Tevatron are thus up to 10% better than those obtained from the LO cross section. If a jet veto is imposed, the limits are almost identical to those found using the LO

TABLE III. Sensitivities achievable at the 95% confidence level for the anomalous $ZZ\gamma$ couplings h_{30}^Z and h_{40}^Z in (a) $pp\to Z\gamma+X\to\ell^+\ell^-\gamma+X$ and (b) $pp\to Z\gamma+X\to\not p_T\gamma+X$, at the LHC ($\sqrt s=14$ TeV). Results are shown for integrated luminosities of 10 fb^{-1} and 100 fb^{-1}. The limits for each coupling apply for arbitrary values of the other coupling listed in this table. The CP violating couplings $h_{1,2}^Z$ and all $Z\gamma\gamma$ couplings are assumed to vanish. For the form factor we use the form of Eq. (4) with $n=3$ ($n=4$) for h_3^Z (h_4^Z) and $\Lambda_{FF}=3$ TeV. The cuts summarized in Sec. III B are imposed. For the jet definition, we have used Eq. (10).

(a) $pp\to Z\gamma+X\to\ell^+\ell^-\gamma+X$			
$\int\mathcal{L}dt=10$ fb^{-1}			
Coupling	LO	NLO incl.	NLO 0-jet
$|h_{30}^Z|$	4.6×10^{-3}	5.0×10^{-3}	4.7×10^{-3}
$|h_{40}^Z|$	3.6×10^{-5}	3.9×10^{-5}	3.7×10^{-5}
$\int\mathcal{L}dt=100$ fb^{-1}			
Coupling	LO	NLO incl.	NLO 0-jet
$|h_{30}^Z|$	2.5×10^{-3}	2.8×10^{-3}	2.6×10^{-3}
$|h_{40}^Z|$	1.7×10^{-5}	1.9×10^{-5}	1.8×10^{-5}
(b) $pp\to Z\gamma+X\to\not p_T\gamma+X$			
$\int\mathcal{L}dt=10$ fb^{-1}			
Coupling	LO	NLO incl.	NLO 0-jet
$|h_{30}^Z|$	3.4×10^{-3}	3.7×10^{-3}	3.5×10^{-3}
$|h_{40}^Z|$	2.5×10^{-5}	2.7×10^{-5}	2.6×10^{-5}
$\int\mathcal{L}dt=100$ fb^{-1}			
Coupling	LO	NLO incl.	NLO 0-jet
$|h_{30}^Z|$	1.9×10^{-3}	2.0×10^{-3}	1.9×10^{-3}
$|h_{40}^Z|$	1.2×10^{-5}	1.3×10^{-5}	1.2×10^{-5}

calculation. In its $p\bar p\to Z\gamma\to\not p_T\gamma$ analysis, the D0 Collaboration imposes a $p_T(j)<15$ GeV requirement, and uses the calculation of Ref. [10] where the effect of the NLO QCD corrections is approximated by a simple k-factor to extract sensitivity limits. We found that the bounds obtained from the full NLO $Z(\to\bar\nu\nu)\gamma+0$ jet calculation are 4–6% weaker than those derived using the calculation used in the experimental analysis.

At the LHC, qg fusion significantly contributes to $Z\gamma$ production and the change in the slope of the $p_T(\gamma)$ distribution caused by the NLO QCD corrections is quite pronounced. As a result, the limits on $ZZ\gamma$ and $Z\gamma\gamma$ couplings extracted from the inclusive NLO $Z\gamma+X$ cross section are up to 10% weaker than those extracted using the LO calculation. The size of the QCD corrections at large photon transverse momenta can be reduced considerably, and a fraction of the sensitivity to $Z\gamma$ couplings which was lost at the LHC may be regained by imposing a jet veto. The improvement, however, is moderate.

Although a jet veto does not have a large effect on the sensitivity bounds at the Tevatron or the LHC, extracting limits from the $Z\gamma+0$ jet channel has the advantage of a reduced uncertainty from the variation of the factorization scale Q^2; the dependence of the NLO $Z\gamma+0$ jet cross section on Q^2 is significantly smaller than that of the inclusive

NLO and the LO $Z\gamma$ cross section.

The effect of QCD corrections on the sensitivity limits for anomalous gauge boson couplings in $Z\gamma$ production is significantly smaller than for $W\gamma$, WZ, and W^+W^- production. In $W\gamma$ and WZ production, the SM Born cross section is suppressed due to the appearance of an exact or approximate radiation zero [42,43]. In W^+W^- production, the strong correlation of the W helicities in the SM, together with the effect of kinematic cuts, is responsible for the larger effect of the QCD corrections [19].

[1] CDF Collaboration, F. Abe *et al.*, Phys. Rev. Lett. **74**, 1936 (1995); D. Benjamin, in *Proceedings of the ''10th Topical Workshop on Proton Antiproton Collider Physics,''* Fermilab, 1995, edited by R. Raja and J. Yoh (AIP Press, New York, 1996), p. 370.

[2] D0 Collaboration, S. Abachi *et al.*, Phys. Rev. Lett. **75**, 1034 (1995); **78**, 3634 (1997).

[3] CDF Collaboration, F. Abe *et al.*, Phys. Rev. Lett. **75**, 1017 (1995); **78**, 4536 (1997).

[4] D0 Collaboration, S. Abachi *et al.*, Phys. Rev. Lett. **750**, 1023 (1995); **77**, 3303 (1996); D0 Collaboration, B. Abbott *et al.*, *ibid.* **79**, 1441 (1997).

[5] D0 Collaboration, S. Abachi *et al.*, Phys. Rev. D **56**, 6742 (1997).

[6] T. Yasuda, FERMILAB-Conf-97/206-E (Report, June 1997), to appear in the e - proceedings of the ''Hadron Collider Physics XII'' Conference, Stony Brook, NY, 1997.

[7] CDF Collaboration, F. Abe *et al.*, Phys. Rev. Lett. **74**, 1941 (1995); D. Neuberger, *Proceedings of the ''International Europhysics Conference on High Energy Physics,''* Brussels, Belgium, 1995, edited by J. Lemonne, C. vander Velde, and F. Verbeure (World Scientific, Singapore, 1996), p. 54.

[8] D0 Collaboration, S. Abachi *et al.*, Phys. Rev. Lett. **75**, 1028 (1995); in Contributed paper to the XXVIIIth International Conference on High Energy Physics, Warsaw, Poland, 1996.

[9] D0 Collaboration, S. Abachi *et al.*, Phys. Rev. Lett. **78**, 3640 (1997).

[10] U. Baur and E. L. Berger, Phys. Rev. D **47**, 4889 (1993).

[11] J. Ohnemus, Phys. Rev. D **47**, 940 (1993).

[12] J. Ohnemus, Phys. Rev. D **51**, 1068 (1995).

[13] H. Baer, J. Ohnemus, and J. F. Owens, Phys. Rev. D **40**, 2844 (1989); **42**, 61 (1990); Phys. Lett. B **234**, 127 (1990); J. Ohnemus and J. F. Owens, Phys. Rev. D **43**, 3626 (1991); J. Ohnemus, *ibid.* **44**, 1403 (1991); **44**, 3477 (1991); H. Baer and M. H. Reno, *ibid.* **43**, 2892 (1991); B. Bailey, J. Ohnemus, and J. F. Owens, *ibid.* **46**, 2018 (1992); J. Ohnemus, *ibid.* **47**, 940 (1993); J. Ohnemus and W. J. Stirling, *ibid.* **47**, 2722 (1993); H. Baer, B. Bailey, and J. F. Owens, *ibid.* **47**, 2730 (1993); L. Bergmann, Ph.D. dissertation, Florida State University, 1989 (unpublished).

[14] R. Barbieri, H. Harari, and M. Leurer, Phys. Lett. **141B**, 455 (1985).

[15] V. Constantini, B. de Tollis, and G. Pistoni, Nuovo Cimento A **2**, 733 (1971); E. W. N. Glover and J. J. van der Bij, Phys. Lett. B **206**, 701 (1988).

[16] U. Baur, T. Han, and J. Ohnemus, Phys. Rev. D **48**, 5140 (1993).

[17] U. Baur, T. Han, and J. Ohnemus, Phys. Rev. D **51**, 3381 (1995).

[18] S. Frixione, P. Nason, and G. Ridolfi, Nucl. Phys. **B383**, 3 (1992).

[19] U. Baur, T. Han, and J. Ohnemus, Phys. Rev. D **53**, 1098 (1996).

[20] S. Frixione, Nucl. Phys. **B410**, 280 (1993).

[21] J. F. Owens, Rev. Mod. Phys. **59**, 465 (1987).

[22] G.'t Hooft and M. Veltman, Nucl. Phys. **B44**, 189 (1972).

[23] U. Baur, E. W. N. Glover, and J. J. van der Bij, Nucl. Phys. **B318**, 106 (1989); V. Barger, T. Han, J. Ohnemus, and D. Zeppenfeld, Phys. Rev. D **41**, 2782 (1990).

[24] K. Hagiwara, R. D. Peccei, D. Zeppenfeld, and K. Hikasa, Nucl. Phys. **B282**, 253 (1987).

[25] C. N. Yang, Phys. Rev. **77**, 242 (1950).

[26] A. Barroso, F. Boudjema, J. Cole, and N. Dombey, Z. Phys. C **28**, 1479 (1985).

[27] J. M. Cornwall, D. N. Levin, and G. Tiktopoulos, Phys. Rev. Lett. **30**, 1268 (1973); Phys. Rev. D **10**, 1145 (1974); C. H. Llewellyn Smith, Phys. Lett. B **46**, 233 (1973); S. D. Joglekar, Ann. Phys. (N.Y.) **83**, 427 (1974).

[28] L3 Collaboration, M. Acciarri *et al.*, Phys. Lett. B **346**, 190 (1995); *ibid.* **412**, 201 (1997).

[29] DELPHI Collaboration, T. Bowcock *et al.*, DELPHI 97-113 CONF 95, paper submitted to the HEP'97 Conference, Jerusalem, 1997.

[30] P. Breitenlohner and D. Maison, Commun. Math. Phys. **52**, 11 (1977); M. Veltman, Nucl. Phys. **B319**, 253 (1989).

[31] J.A.M. Vermaseren, FORM User's Manual, NIKHEF-H, Amsterdam, 1989.

[32] CDF Collaboration, F. Abe *et al.*, Phys. Rev. Lett. **73**, 225 (1994); Phys. Rev. D **50**, 2966 (1994); Phys. Rev. Lett. **74**, 2626 (1995); Report No. FERMILAB-Pub-97/284-E, 1997 (unpublished); Report No. FERMILAB-Pub-97/304-E, 1997 (unpublished).

[33] D0 Collaboration, S. Abachi *et al.*, Phys. Rev. Lett. **74**, 2422 (1995); **74**, 2632 (1995); Phys. Rev. D **52**, 4877 (1995); Phys. Rev. Lett. **79**, 1197 (1997); D0 Collaboration, B. Abbott *et al.*, Report No. FERMILAB-Pub-97/172-E, 1997 (unpublished); R. Raja, Report No. FERMILAB-Conf-97/194-E, 1997.

[34] R. G. Wagner, FERMILAB-Conf/97-302-E, to appear in the Proceedings of the ''5th International Conference on Physics Beyond the Standard Model,'' Balholm, Norway, 1997; LEP Electroweak Working Group, D. Abbaneo *et al.*, Report No.

CERN-PPE/96-183, 1996 (unpublished).

[35] W. A. Bardeen, A. J. Buras, D. W. Duke, and T. Muta, Phys. Rev. D **18**, 3998 (1978).

[36] A. D. Martin, R. G. Roberts, and W. J. Stirling, Phys. Rev. D **50**, 6734 (1994).

[37] J. Ohnemus and W. J. Stirling, Phys. Lett. B **298**, 230 (1993).

[38] P. Aurenche, R. Baier, and M. Fontannaz, Phys. Rev. D **42**, 1440 (1990); P. Aurenche *et al.*, in *Proceedings of the Large Hadron Collider Workshop*, Aachen, Germany, 1990, edited by G. Jarlskog and D. Rein, CERN 90-10, Vol. II, p. 69; CDF Collaboration, F. Abe *et al.*, Phys. Rev. Lett. **68**, 2734 (1992).

[39] CMS Collaboration, M. Della Negra *et al.*, CMS Letter of Intent, CERN-LHCC-92-3, 1992 (unpublished); CMS Collaboration, G. L. Bayatian *et al.*, CMS Technical Design Report, CERN-LHCC-94-38, 1994 (unpublished).

[40] ATLAS Collaboration, D. Gingrich *et al.*, ATLAS Letter of Intent, CERN-LHCC-92-4, 1992 (unpublished); ATLAS Collaboration, W. W. Armstrong *et al.*, ATLAS Technical Design Report, CERN-LHCC-94-43, 1994 (unpublished).

[41] CDF Collaboration, F. Abe *et al.*, Phys. Rev. D **45**, 3921 (1992).

[42] R. W. Brown, K. O. Mikaelian, and D. Sahdev, Phys. Rev. D **20**, 1164 (1979); K. O. Mikaelian, M. A. Samuel, and D. Sahdev, Phys. Rev. Lett. **43**, 746 (1979).

[43] U. Baur, T. Han, and J. Ohnemus, Phys. Rev. Lett. **72**, 3941 (1994).

[44] G. Ciapetti and A. Di Ciaccio, Proceedings of the ECFA Workshop on LHC Physics, Aachen, FRG, 1990, Vol. II, p. 155.

[45] J. P. Marriner, in Proceedings of the Workshop ''New Directions in High Energy Physics,'' Snowmass, CO, 1996, edited by D.G. Cassel, L. Trindle Gennari, and R.H. Siemann, Vol. 1, p. 78; P. P. Bagley *et al.*, *ibid.*, Vol. 1, p. 134; D. A. Finley, J. Marriner, and N. V. Mokhov, FERMILAB-Conf-96/408, presented at the ''Conference on Charged Particle Accelerators,'' Protvino, Russia, 1996 (unpublished).

[46] The LHC Study Group, D. Bousard *et al.*, CERN/AC/95-05, 1995 (unpublished).

[47] P. Arnold and R. Kauffman, Nucl. Phys. **B349**, 381 (1991); R. Kauffman, Phys. Rev. D **44**, 1415 (1991); Phys. Rev. D **45**, 1512 (1992); T. Han, R. Meng, and J. Ohnemus, Nucl. Phys. **B384**, 59 (1992); C. P. Yuan, Phys. Lett. B **283**, 395 (1992); C. Balazs and C. P. Yuan, Phys. Rev. D **56**, 5558 (1997); R. K. Ellis, D. A. Ross, and S. Veseli, Nucl. Phys. **B503**, 309 (1997); R. K. Ellis and S. Veseli, FERMILAB-Pub/97-207-T.

[48] G. Landsberg, Proceedings of the Workshop on Physics at Current Accelerators and Supercolliders, Argonne, Illinois, 1993, edited by J. L. Hewett, A. R. White, and D. Zeppenfeld, p. 303.